

IDENTIFYING THE LIGHTS POSITION IN PHOTOMETRIC STEREO UNDER UNKNOWN LIGHTING

A.CONCAS*, R. DESSÌ†, C. FENU*, G. RODRIGUEZ*, AND M. VANZI†

Abstract. Reconstructing the 3D shape of an object from a set of images is a classical problem in Computer Vision. Photometric stereo is one of the possible approaches. It stands on the assumption that the object is observed from a fixed point of view under different lighting conditions. The traditional approach requires that the position of the light sources is accurately known. It has been proved that the lights position can be estimated directly from the data when at least 6 images of the observed object are available. In this paper, we present a Matlab implementation of the algorithm for solving the photometric stereo problem under unknown lighting, and propose a simple shooting technique to solve the bas-relief ambiguity.

Key words. photometric stereo, low-rank approximation, finite differences, shape from shading, computer vision.

1. Introduction. *Shape from shading* is a typical problem in Computer Vision [17, 18, 26]. It exploits shading information for recovering the 3D shape of an object from a set of discretized 2D projections (e.g., digital pictures), when the object is illuminated by a single light source. If only one picture is available, the *shape from shading* problem is not well posed, as its solution is not unique. A way to solve this problem and remove the uncertainty is to use more than one image. There are two main possible approaches to the problem. Stereo vision, sometimes generalized to multiple views vision or *multiview* [13], assumes the availability of different observations of an object obtained by varying the point of view, but not the illumination. The pictures are typically obtained by a set of fixed cameras, or extracted from the frames of a movie shot by a moving camera. Photometric stereo (PS) [29] is a *shape from shading* method that uses a fixed camera and a movable light to acquire a set of images that embed shape and color (albedo) information of the framed object [10]. The ideal PS requires the lights position and intensity to be accurately known [3], a deviation from this requirement often results in a distorted reconstruction.

Various attempts have been made to estimate the lights position directly from the data; see, e.g., [4, 9] where a linear combination of special functions (spherical harmonics) is employed. The problem was solved in [16], where it was shown that at least 6 images under different lighting conditions are needed. Such a result releases the constraint on the precise positioning of the light sources, making the acquisition process much simpler.

We devoted various papers to the application of photometric stereo to rock art documentation, in particular to the 3D reconstruction of the decorations found in the “Domus de Janas”, a particular kind of Neolithic tombs typical of Sardinia, Italy [12, 21, 22, 28]. Some B.S. students were also involved in this study [11, 14, 20, 27]. In the archaeology setting, a 3D restoration technique based on easy data acquisition is crucial, because the findings are frequently located in uncomfortable positions and the current protocols exclude any physical contact for creating replicas. The difficulty to access specific sites, often associated to a large number of items to be documented, makes it impractical to use other 3D reconstruction techniques, like laser scanning, characterized by long acquisition time and large instrumentation cost. Indeed, cheap instrumentation would allow for parallel operation on different findings by a team of researchers.

In this paper we present a Matlab implementation for the solution of the photometric stereo problem under unknown lighting. First, the normal vector field is determined by a technique due to Hayakawa [16], which can estimate the lights position directly from the data when at least 6 images of the observed object are available. Then, an explicit representation of the observed surface, based on an orthographic projection, is obtained by integrating the normal field. This is done by solving a Poisson equation with either Dirichlet or Neumann boundary conditions. Finally, we propose a practical shooting procedure to circumvent the well known bas-relief ambiguity [5],

*Department of Mathematics and Computer Science, University of Cagliari, viale Merello 92, 09123 Cagliari, Italy. E-mail: anna.concas@unica.it, kate.fenu@unica.it, rodriguez@unica.it.

†Department of Electrical and Electronic Engineering, University of Cagliari, Piazza D’Armi, 09123 Cagliari, Italy. E-mail: richidessi@gmail.com, vanzi@diee.unica.it.

and demonstrate the performance of the developed software on both synthetic and experimental data sets.

Section 2 introduces the notation adopted in the paper, while Section 3 resumes the solution of the problem when the lights position is known in advance. Photometric stereo under unknown lighting is studied in Section 4, where we recall a theorem which gives sufficient conditions for the existence of the solution. Section 5 illustrates a procedure for determining the right orientation of the surface. A selection of numerical results are illustrated in Section 6, and Section 7 describes possible future developments.

2. Notation. Let us consider an object placed at the origin of a reference system in \mathbb{R}^3 . The object is observed from a fixed camera, the z -axis coincides with the optical axis and it is directed from the object to the camera. The point of view is assumed to be at infinite distance from the observed object (ortographic projection), and different pictures of the object are taken, each one with a different light direction. Each image has resolution $(r + 2) \times (s + 2)$, and the real length of the horizontal side of each image is A . Assuming the pixels to be square, we let the length of the vertical side be $B = (s + 1)h$, with $h = A/(r + 1)$. Each picture defines a domain $\Omega = [-A/2, A/2] \times [-B/2, B/2]$, and induces the discretization

$$\begin{aligned} x_i &= -A/2 + ih, & i &= 0, \dots, r + 1, \\ y_j &= -B/2 + jh, & j &= 0, \dots, s + 1. \end{aligned} \tag{2.1}$$

We let the surface of the object be represented by $z = u(x, y)$, with $(x, y) \in \Omega$. Then,

$$\nabla u(x, y) = \begin{bmatrix} \frac{\partial u(x, y)}{\partial x} \\ \frac{\partial u(x, y)}{\partial y} \end{bmatrix} = \begin{bmatrix} u_x \\ u_y \end{bmatrix}, \quad \mathbf{n}(x, y) = \frac{(-u_x, -u_y, 1)^T}{\sqrt{1 + \|\nabla u\|^2}}, \tag{2.2}$$

denote the gradient of u and the normal vector to the surface of the object, respectively.

As it is customary, images are vectorized by ordering the pixels lexicographically. The pixel of coordinates (i, j) takes the index $k = (i - 1)s + j$, where $k = 1, \dots, p$, and p is the number of pixels in the image. We will set either $p = (r + 2)(s + 2)$ or $p = rs$ depending on whether the boundary pixels are considered in the discretization or not. For each point in the discretization of Ω , we write indifferently

$$\begin{aligned} u(x_i, y_j) &= u_{i,j} = u_k, \\ u_x(x_i, y_j) &= (u_x)_{i,j} = (u_x)_k, \\ u_y(x_i, y_j) &= (u_y)_{i,j} = (u_y)_k, \\ \mathbf{n}(x_i, y_j) &= \mathbf{n}_{i,j} = \mathbf{n}_k, \end{aligned}$$

using the two-index notation to refer to the values on the grid, and the one-index notation to identify the values after the vectorization.

We assume that q pictures are available, each one with light source at infinite distance from the origin along the direction

$$\boldsymbol{\ell}_t = \begin{pmatrix} \ell_{1t} \\ \ell_{2t} \\ \ell_{3t} \end{pmatrix}, \quad t = 1, \dots, q.$$

Each vector $\boldsymbol{\ell}_t$ stems from the object to the light source and its Euclidean norm is proportional to the light intensity. This introduces an undetermined proportionality constant in the problem. The image vectors are denoted by $\mathbf{m}_1, \mathbf{m}_2, \dots, \mathbf{m}_q \in \mathbb{R}^p$. The aim is to reconstruct the 3D shape of the object.

3. Photometric stereo with known lighting. If the surface of the object is *Lambertian* [18], then the light intensity observed at each point is proportional to the angle between the normal to the observed surface at that point and the light direction. This model is usually referred to as Lambert’s cosine law. It can be stated as

$$\rho(x, y) \langle \mathbf{n}(x, y), \boldsymbol{\ell}_t \rangle = \mathcal{I}_t(x, y), \quad t = 1, \dots, q \quad (3.1)$$

where the scalar function $\rho(x, y)$ represents the *albedo* at each surface point and it keeps into account the partial light absorption of that portion of the surface. The light intensity at each point of the t th image is denoted by $\mathcal{I}_t(x, y)$, and $\langle \cdot, \cdot \rangle$ is the usual inner product in \mathbb{R}^3 . When the albedo is constant, the object is said to be a *Lambertian reflector*.

Summing up, the classical assumptions for this model are the following:

- the surface is Lambertian;
- the light sources are placed at infinite distance;
- no portion of the surface is shaded in all the pictures;
- the camera is sufficiently far from the object so that perspective deformations can be neglected.

In this section, we assume that the light directions $\boldsymbol{\ell}_t$, $t = 1, \dots, q$, are known.

The continuous formulation (3.1) of Lambert’s law leads to a Hamilton–Jacobi differential model; see [24, 25] for a thorough study. Here we briefly review its construction.

Setting

$$\boldsymbol{\ell}_t = \begin{pmatrix} \tilde{\boldsymbol{\ell}}_t \\ \ell_{3t} \end{pmatrix}, \quad \tilde{\boldsymbol{\ell}}_t \in \mathbb{R}^2,$$

equation (3.1) becomes

$$\rho(x, y) \frac{\langle -\nabla u(x, y), \tilde{\boldsymbol{\ell}}_t \rangle + \ell_{3t}}{\sqrt{1 + \|\nabla u(x, y)\|^2}} = \mathcal{I}_t(x, y), \quad t = 1, \dots, q,$$

or, equivalently,

$$\mathcal{I}_t(x, y) \sqrt{1 + \|\nabla u(x, y)\|^2} + \rho(x, y) (\langle \nabla u(x, y), \tilde{\boldsymbol{\ell}}_t \rangle - \ell_{3t}) = 0.$$

By imposing Dirichlet boundary conditions, one obtains the system of q first order nonlinear PDEs of Hamilton–Jacobi type

$$\begin{cases} H_t(x, y, \nabla u(x, y)) = 0, & t = 1, \dots, q, \\ u(x, y) = g(x, y), & (x, y) \in \partial\Omega. \end{cases}$$

Following [25], we obtain for $t = 1$

$$\sqrt{1 + \|\nabla u(x, y)\|^2} = \rho(x, y) \frac{\langle -\nabla u(x, y), \tilde{\boldsymbol{\ell}}_1 \rangle + \ell_{31}}{\mathcal{I}_1(x, y)}$$

and we substitute this expression in the equations corresponding to $t = 2, \dots, q$, to obtain

$$\left(\langle -\nabla u(x, y), \tilde{\boldsymbol{\ell}}_1 \rangle - \ell_{31} \right) \mathcal{I}_t(x, y) = \left(\langle -\nabla u(x, y), \tilde{\boldsymbol{\ell}}_t \rangle - \ell_{3t} \right) \mathcal{I}_1(x, y).$$

This shows that the minimal number of images for the problem to be well-posed is 2. Nevertheless, if $q = 2$ the solution may not exist for particular light orientations. Considering $q > 2$ leads to a least-squares approach, that may be effective to reduce the influence of noise in experimental data sets, without making data acquisition significantly harder. In any case, knowing accurately the lights position $\boldsymbol{\ell}_t$ is a strong requirement.

After $u(x, y)$ is computed, the albedo is given by

$$\rho(x, y) = \frac{\mathcal{I}_t(x, y)}{\langle \mathbf{n}(x, y), \boldsymbol{\ell}_t \rangle}, \quad \text{for any } t = 1, \dots, q.$$

Conditions for the existence of solutions are discussed in [19], and in [25] the problem is studied under more realistic assumptions; see also [27].

The main disadvantage of the Hamilton–Jacobi model is that the operator to be inverted depends upon the data. The matrix of the linear system obtained through the discretization may be singular or severely ill-conditioned in certain lighting conditions. However, this problem can be tackled by suitably choosing the position of the light sources.

An alternative approach for the 3D reconstruction of a Lambertian surface is based on splitting the computation into two subproblems, one concerning the computation of the normal vectors and another in the reconstruction of the surface by the solution of a Poisson equation.

The first step consists of immediately discretizing Lambert’s law on a regular grid, and determining the normal vector field to the surface by solving a matrix equation. This operation is mostly influenced by the lights position, Then, the divergence of the normal field is numerically approximated, to obtain a discretization of the Laplace operator, and the 3D profile of the observed object is recovered by solving a Poisson partial differential equation. This part is uniquely concerned with the camera position.

The advantages of this approach are that the computation is decoupled into simpler problems, and that it allows for the solution of the unknown lighting case, as it will be shown in the next section. A drawback is that this procedure requires a larger number of images than the Hamilton–Jacobi formulation, i.e., at least 3. This is not a substantial problem in applications, since usually dozens of images can be easily made available.

Let us apply discretization (2.1) to equation (3.1). We ignore for the moment the boundary pixels, where we will impose suitable boundary conditions, and rearrange the internal pixels by the lexicographical ordering. Denoting by ρ_k and \mathbf{n}_k , respectively, the value of the albedo and the (normalized) normal vector to the surface at the k th pixel, then the following relation holds at each point of each picture

$$\rho_k \mathbf{n}_k^T \boldsymbol{\ell}_t = m_{kt}, \quad k = 1, \dots, p, \quad t = 1, \dots, q. \quad (3.2)$$

The scalars m_{kt} represent the radiation $\mathcal{I}_t(x, y)$ reflected by the small area near the k th pixel when illuminated from the direction $\boldsymbol{\ell}_t$, that is, the components of the vectors $\mathbf{m}_1, \mathbf{m}_2, \dots, \mathbf{m}_q \in \mathbb{R}^p$, containing the vectorized images.

By defining the matrices

$$\begin{aligned} D &= \text{diag}(\rho_1, \dots, \rho_p) \in \mathbb{R}^{p \times p}, \\ L &= [\boldsymbol{\ell}_1, \dots, \boldsymbol{\ell}_q] \in \mathbb{R}^{3 \times q}, \\ N &= [\mathbf{n}_1, \dots, \mathbf{n}_p] \in \mathbb{R}^{3 \times p}, \\ M &= [\mathbf{m}_1, \dots, \mathbf{m}_q] \in \mathbb{R}^{p \times q}, \end{aligned}$$

the equations (3.2) can be grouped into the matrix equation

$$DN^T L = M. \quad (3.3)$$

When the lights positions are known, we first compute

$$\tilde{N}^T = ML^\dagger, \quad (3.4)$$

where L^\dagger is the Moore–Penrose pseudoinverse of L [6]. Then, the matrices D and N , defining the albedo and the normal vectors, can be computed from the factorization $ND = \tilde{N}$ by simply normalizing the columns of \tilde{N} .

For the solution of (3.4) to be unique, it is necessary that $q \geq 3$, from which we see that the minimum number of images required to obtain the normal field by this approach is 3.

Once the field of the normal vectors to the surface is obtained, we consider the vectors

$$((u_x)_k, (u_y)_k, -1)^T = -\frac{\mathbf{n}_k}{(\mathbf{n}_k)_3},$$

obtained by normalizing to -1 the third component of the normals \mathbf{n}_k ; see (2.2). We numerically differentiate the first two components of the above vectors to obtain an approximation on the grid (2.1) of the Laplacian $f(x, y) = u_{xx} + u_{yy}$. To do that, we employ the following formula, based on the second order centered finite differences approximation for the first derivative

$$f_{i,j} = f(x_i, y_j) \approx \frac{(u_x)_{i+1,j} - (u_x)_{i-1,j}}{2h} + \frac{(u_y)_{i,j+1} - (u_y)_{i,j-1}}{2h}. \quad (3.5)$$

Then, the 3D profile of the object, represented by the explicit function $z = u(x, y)$, can be recovered by solving the Poisson partial differential equation

$$\Delta u(x, y) = f(x, y), \quad (3.6)$$

where Δ denotes the Laplace operator, and suitable boundary condition must be imposed to ensure unicity of solution.

We discretize the Poisson equation by a second order finite differences scheme and initially consider Dirichlet boundary conditions. Consider the equation (3.6) on the rectangle $[-A/2, A/2] \times [-B/2, B/2]$, with boundary conditions

$$\begin{aligned} u(x, -B/2) &= \phi_1(x), & u(x, B/2) &= \phi_2(x), & x &\in [-A/2, A/2], \\ u(-A/2, y) &= \psi_1(y), & u(A/2, y) &= \psi_2(y), & y &\in [-B/2, B/2]. \end{aligned}$$

Let $u(x_i, y_j) = u_{i,j}$ and $f(x_i, y_j) = f_{i,j}$ at each point of the mesh (2.1). Then, the boundary values are denoted by $u_{i,0} = \phi_1(x_i)$, $u_{i,s+1} = \phi_2(x_i)$, $u_{0,j} = \psi_1(y_j)$, and $u_{r+1,j} = \psi_2(y_j)$.

Discretizing the Poisson equation by the well-known five point scheme with stepsize h , we obtain the linear system

$$u_{i-1,j} + u_{i,j-1} - 4u_{i,j} + u_{i,j+1} + u_{i+1,j} = \tilde{f}_{i,j}, \quad (3.7)$$

for $i = 1, \dots, r$ and $j = 1, \dots, s$, with $\tilde{f}_{i,j} = h^2 f_{i,j}$. We remark that approximating $f_{i,j}$ by (3.5) does not deteriorate the quality of the results, as both (3.5) and the five point scheme produce an approximation of order $O(h^2)$. This assertion has been verified numerically.

By aggregating the mesh points $u_{i,j}$ by columns, we obtain the following pentadiagonal system of size $p = rs$

$$\begin{cases} T\mathbf{u}_1 + I_s\mathbf{u}_2 & = \mathbf{b}_1, \\ I_s\mathbf{u}_{i-1} + T\mathbf{u}_i + I_s\mathbf{u}_{i+1} & = \mathbf{b}_i, & i = 2, \dots, r-1, \\ I_s\mathbf{u}_{r-1} + T\mathbf{u}_r & = \mathbf{b}_r, \end{cases} \quad (3.8)$$

where I_s denotes the identity matrix of size s ,

$$T = \begin{bmatrix} -4 & 1 & & & \\ 1 & -4 & \ddots & & \\ & \ddots & \ddots & \ddots & \\ & & & 1 & -4 \end{bmatrix} \in \mathbb{R}^{s \times s}, \quad \mathbf{u}_i = \begin{bmatrix} u_{i,1} \\ u_{i,2} \\ \vdots \\ u_{i,s} \end{bmatrix} \in \mathbb{R}^s, \quad i = 1, \dots, r.$$

The right-hand side vectors are

$$\mathbf{b}_1 = \begin{bmatrix} \tilde{f}_{1,1} \\ \tilde{f}_{1,2} \\ \vdots \\ \tilde{f}_{1,s} \end{bmatrix} - \begin{bmatrix} u_{0,1} + u_{1,0} \\ u_{0,2} \\ \vdots \\ u_{0,s} + u_{1,s+1} \end{bmatrix},$$

$$\mathbf{b}_r = \begin{bmatrix} \tilde{f}_{r,1} \\ \tilde{f}_{r,2} \\ \vdots \\ \tilde{f}_{r,s} \end{bmatrix} - \begin{bmatrix} u_{r+1,1} + u_{r,0} \\ u_{r+1,2} \\ \vdots \\ u_{r+1,s} + u_{r,s+1} \end{bmatrix},$$

and

$$\mathbf{b}_i = \begin{bmatrix} \tilde{f}_{i,1} \\ \tilde{f}_{i,2} \\ \vdots \\ \vdots \\ \tilde{f}_{i,s} \end{bmatrix} - \begin{bmatrix} u_{i,0} \\ 0 \\ \vdots \\ 0 \\ u_{i,s+1} \end{bmatrix} \in \mathbb{R}^s, \quad i = 2, \dots, r-1.$$

The system has the condensed representation $\mathbf{A}\mathbf{u} = \mathbf{b}$, where

$$\mathbf{u} = \begin{bmatrix} \mathbf{u}_1 \\ \mathbf{u}_2 \\ \vdots \\ \vdots \\ \mathbf{u}_r \end{bmatrix} \in \mathbb{R}^p, \quad \mathbf{b} = \begin{bmatrix} \mathbf{b}_1 \\ \mathbf{b}_2 \\ \vdots \\ \mathbf{b}_{r-1} \\ \mathbf{b}_r \end{bmatrix} \in \mathbb{R}^p,$$

and

$$A = \begin{bmatrix} T & I_s & & & \\ I_s & T & \ddots & & \\ & \ddots & \ddots & \ddots & \\ & & & I_s & T \end{bmatrix} \in \mathbb{R}^{p \times p}.$$

This square linear system of size p (number of pixels) can be solved by any general direct or preconditioned iterative method suited for large sparse matrices [15], or, specifically, by a fast Poisson solver [7, 8].

In practical photometric stereo, one usually focuses on the case of homogeneous Dirichlet boundary conditions, i.e., $\phi_1(x) = \phi_2(x) = \psi_1(y) = \psi_2(y) = 0$, which corresponds to assuming that the observed object stands on a flat background.

When the value of the function $u(x, y)$ on the boundary is unknown, there may be information on the normal derivatives of the solution. This amounts to imposing the following Neumann boundary conditions on the horizontal and vertical boundaries of the domain

$$-\frac{\partial u(x, -B/2)}{\partial y} = \mu_1(x), \quad \frac{\partial u(x, B/2)}{\partial y} = \mu_2(x), \quad (3.9)$$

$$-\frac{\partial u(-A/2, y)}{\partial x} = \nu_1(y), \quad \frac{\partial u(A/2, y)}{\partial x} = \nu_2(y). \quad (3.10)$$

Neumann boundary conditions are not sufficient to make the problem well posed. In fact, the solution is determined up to an additive constant, so the slope of a point of the solution has to be fixed arbitrarily.

In this case, the solution at the boundary is to be determined too, and the number of unknowns $u_{i,j}$ increases from rs to $p = (r+2)(s+2)$. Equation (3.7) is still valid for all the internal points of the grid, that is, for $i = 1, \dots, r$ and $j = 1, \dots, s$, but it has to be coupled to the discretization of the conditions (3.9) and (3.10). To do this, we employed a one-sided second order discretization, obtaining on the horizontal boundaries of the domain

$$\begin{aligned} 3u_{i,0} - 4u_{i,1} + u_{i,2} &= \tilde{\mu}_{1,i}, \\ u_{i,s-1} - 4u_{i,s} + 3u_{i,s+1} &= \tilde{\mu}_{2,i}, \end{aligned}$$

with $\tilde{\mu}_{1,i} = 2h\mu_1(x_i)$ and $\tilde{\mu}_{2,i} = 2h\mu_2(x_i)$, for $i = 1, \dots, r$. Similarly, on the vertical boundaries, we get

$$\begin{aligned} 3u_{0,j} - 4u_{1,j} + u_{2,j} &= \tilde{\nu}_{1,j}, \\ u_{r-1,j} - 4u_{r,j} + 3u_{r+1,j} &= \tilde{\nu}_{2,j}, \end{aligned}$$

with $\tilde{\nu}_{1,j} = 2h\nu_1(y_j)$ and $\tilde{\nu}_{2,j} = 2h\nu_2(y_j)$, for $j = 1, \dots, s$. On the four corner points, we perform a linear interpolation from the three neighbour nodes of the grid. The equation for the corner with coordinates (x_0, y_0) is

$$u_{0,0} - u_{0,1} - u_{1,0} + u_{1,1} = 0.$$

Similar equations correspond to the other three corners of the rectangular domain.

The resulting linear system

$$B\mathbf{u} = \mathbf{c} \tag{3.11}$$

is defined by

$$B = \begin{bmatrix} P & Q & S & & & \\ S & R & S & & & \\ & \ddots & \ddots & \ddots & & \\ & & S & R & S & \\ & & S & Q & P & \end{bmatrix}, \quad \mathbf{u} = \begin{bmatrix} \mathbf{u}_0 \\ \mathbf{u}_1 \\ \vdots \\ \mathbf{u}_r \\ \mathbf{u}_{r+1} \end{bmatrix}, \quad \mathbf{c} = \begin{bmatrix} \mathbf{c}_0 \\ \mathbf{c}_1 \\ \vdots \\ \mathbf{c}_r \\ \mathbf{c}_{r+1} \end{bmatrix},$$

with

$$\begin{aligned} P &= \begin{bmatrix} 1 & -1 & & & & \\ & 3 & & & & \\ & & \ddots & & & \\ & & & 3 & & \\ & & & -1 & 1 & \end{bmatrix}, \\ Q &= \begin{bmatrix} -1 & 1 & & & & \\ & -4 & & & & \\ & & \ddots & & & \\ & & & -4 & & \\ & & & 1 & -1 & \end{bmatrix}, \\ R &= \begin{bmatrix} 3 & -4 & 1 & & & \\ 1 & -4 & 1 & & & \\ & \ddots & \ddots & \ddots & & \\ & & 1 & -4 & 1 & \\ & & 1 & -4 & 3 & \end{bmatrix}, \end{aligned}$$

and $S = \text{diag}(0, 1, \dots, 1, 0)$.

The expression of the right-hand side is the following:

$$\mathbf{c}_0 = \begin{bmatrix} 0 \\ \tilde{\nu}_{1,1} \\ \vdots \\ \tilde{\nu}_{1,s} \\ 0 \end{bmatrix}, \quad \mathbf{c}_{r+1} = \begin{bmatrix} 0 \\ \tilde{\nu}_{2,1} \\ \vdots \\ \tilde{\nu}_{2,s} \\ 0 \end{bmatrix}, \quad \mathbf{c}_i = \begin{bmatrix} \tilde{\mu}_{1,i} \\ \tilde{f}_{i,1} \\ \vdots \\ \tilde{f}_{i,s} \\ \tilde{\nu}_{2,i} \end{bmatrix}, \quad i = 1, \dots, r.$$

REMARK 3.1. To make both the matrix B nonsingular and the solution unique, we substitute in (3.11) the equation associated to a chosen internal point of the domain, say, (x_i, y_j) , with the equation $u_{i,j} = \gamma$, where γ is the slope assigned to that point.

4. Photometric stereo under unknown lighting. The need for an accurate localization of the light sources position is a strong limitation for the practical application of photometric stereo. For this reason, the automatic determination of the light directions has been of interest to many researchers.

Referring to a *4-sources photometric stereo*, some papers conjecture that the problem with unknown lighting can be uniquely solved using only 4 images. In [9] the authors suggest an approach based on the use of low-order spherical harmonics for Lambertian objects, while [4] proposes a method based on the decomposition of the light intensity into a linear combination of spherical harmonics.

The problem was actually solved by Hayakawa in [16]. We briefly review here his results, as they contain the main steps of the numerical procedure. The photometric stereo technique under unknown lighting consists of computing the rank-3 factorization

$$\tilde{N}^T L = M, \tag{4.1}$$

where $\tilde{N} = ND$ (see (3.3)), without knowing in advance the lights location, i.e., the matrix L . This problem has not a unique solution. Nevertheless, there are some physical constraints which allow one to find a meaningful solution.

LEMMA 4.1. *The matrices D , N , and L , containing the albedo, the normals to the observed surface, and the lights directions, are determined up to a unitary transformation, that is, (4.1) is satisfied by the matrix pair $(Q\tilde{N}, QL)$, for any orthogonal matrix $Q \in \mathbb{R}^{3 \times 3}$.*

Proof. Any matrix pair $(A^{-T}\tilde{N}, AL)$, with $A \in \mathbb{R}^{3 \times 3}$ nonsingular, satisfies (4.1). Since the normal vectors \mathbf{n}_k are normalized, the norm of the k th column of \tilde{N} equals the albedo ρ_k , while $\|\ell_t\|$ is proportional to the light intensity. This implies that the transformation matrix A has to be orthogonal. \square

The above Lemma suggests that the original orientation of the observed object cannot be determined without further a priori information. This fact, known as *bas-relief ambiguity* [5], should be expected, since only the relative position between the object and the camera can be deduced from a set of images. This indetermination imposes some care in the shape reconstruction, because there is the possibility of axes reflections in the computation of the solution, which would alter significantly the shape of the reconstructed object. We will treat this particular problem in the next section.

In what follows, it is not restrictive to assume $\|\ell_t\| = 1$, $t = 1, \dots, q$. Indeed, we already noticed that there is an undetermined proportionality constant in the problem, depending upon the unit of measure adopted for light intensity, and in the typical experimental setting the pictures are taken using a flashlight at a fixed distance from the object, which produces a constant light intensity across the observations. In particular situations the light intensity may vary, for example when the size of the observed object requires the use of the sun as a light source, taking pictures at different times of the day. In this case a light meter can be used to obtain an estimate of $\|\ell_t\|$.

Let the ‘‘compact’’ singular value decomposition (SVD) [15] of the observations matrix be

$$M = U\Sigma V^T, \tag{4.2}$$

where $\Sigma = \text{diag}(\sigma_1, \dots, \sigma_q)$ is the diagonal matrix containing the singular values and $U \in \mathbb{R}^{p \times q}$, $V \in \mathbb{R}^{q \times q}$ are matrices whose orthonormal columns \mathbf{u}_i and \mathbf{v}_i are the left and right singular vectors, respectively. In our application $q \ll p$, since the number of pixels in an image is usually very large, while we would like to obtain a reconstruction using a set of observations as small as possible. As we observed in the previous section, it is only required that $q \geq 3$.

When q is small, the SVD factorization can be computed efficiently by standard numerical libraries; we used the `svd` function of Matlab [23] even for a quite large value of p . In particular situations, in order to reduce the computation time, one may compute a partial singular value decomposition by an iterative method; see, e.g., [1, 2].

Since the images may be acquired in non-ideal conditions and may be affected by noise, factorization (4.2) usually has numerical rank $r > 3$. Then, a *truncated SVD* must be performed by setting $\sigma_4 = \dots = \sigma_q = 0$. We let $W = [\sigma_1 \mathbf{u}_1, \sigma_2 \mathbf{u}_2, \sigma_3 \mathbf{u}_3]^T$ and $Z = [\mathbf{v}_1, \mathbf{v}_2, \mathbf{v}_3]^T$, so that $W^T Z \simeq M$. This choice produces the best rank-3 approximation to the data matrix M with respect to both the Euclidean and the Frobenius norm [6]. The constructive proof of the following theorem from [16] shows how to obtain the sought matrices \tilde{N} and L from this initial factorization.

THEOREM 4.2. *The normal vectors to the observed surface and the lights position can be uniquely determined from (3.3), up to a unitary transformation, only if at least 6 images taken in different lighting conditions are available.*

Proof. Let us consider the initial rank-3 factorization $W^T Z = M$ described above, with $W = [\mathbf{w}_1, \dots, \mathbf{w}_p]$ and $Z = [\mathbf{z}_1, \dots, \mathbf{z}_q]$. Given the assumption on the norms of the vectors $\boldsymbol{\ell}_t$, we first determine a matrix B such that $\|B\mathbf{z}_t\| = 1$ for each $t = 1, \dots, q$. This implies solving the system of equations

$$\text{diag}(Z^T G Z) = \mathbf{1}, \quad (4.3)$$

where $\mathbf{1} = (1, \dots, 1)^T \in \mathbb{R}^q$ and $G = B^T B$ is a symmetric positive definite 3×3 matrix. The matrix G depends upon 6 independent parameters, say, its elements g_{ij} with $i \leq j$. As each equation in (4.3) is of the type

$$\mathbf{z}_t^T G \mathbf{z}_t = \sum_{i,j=1}^3 z_{it} z_{jt} g_{ij} = 1,$$

the system (4.3) can be rewritten in the form

$$H \mathbf{g} = \mathbf{1},$$

where $\mathbf{g} = (g_{11}, g_{22}, g_{33}, g_{12}, g_{13}, g_{23})^T$ and H is a $q \times 6$ matrix, whose rows are

$$[z_{1t}^2 \quad z_{2t}^2 \quad z_{3t}^2 \quad 2z_{1t}z_{2t} \quad 2z_{1t}z_{3t} \quad 2z_{2t}z_{3t}], \quad t = 1, \dots, q.$$

A necessary condition for the solution vector \mathbf{g} to be unique is that $q \geq 6$. This completes the proof. \square

REMARK 4.1. The above theorem shows that at least 6 images are needed to reconstruct a shape by photometric stereo under unknown lighting. This is only a necessary condition for the unique solvability of the problem, as H may be rank-deficient even for $q \geq 6$. In fact, the requirement on the rank of H poses some constraints on the lights disposition. For example, a very common experimental approach is to place the light sources roughly on a circle around the camera, i.e., at a fixed distance δ from the origin, on a plane parallel to the observation plane. This is equivalent to fixing angles $\theta_1, \dots, \theta_q \in [0, 2\pi)$ and setting

$$\boldsymbol{\ell}_t = \frac{(\cos \theta_t, \sin \theta_t, \delta)^T}{\sqrt{1 + \delta^2}}, \quad t = 1, \dots, q.$$

This lights placement is not acceptable, because in this case the third column of the matrix H would be a linear combination of the first two. So at least one light source should violate this

scheme. Placing the light sources at random positions around the object is often a safe and easy way to ensure that H is full-rank.

As the sought matrix B is determined up to a unitary transformation, we represent it by its QR factorization $B = QR$. The “essential” factor R can be obtained by the Cholesky factorization $G = R^T R$ [15], while Q cannot be uniquely determined; see Lemma 4.1. We will discuss a reasonable choice for the matrix Q in the following section.

Once Q is determined, problem (4.1) is solved by setting

$$\tilde{N} = QR^{-T}W \quad \text{and} \quad L = QRZ. \quad (4.4)$$

By normalizing the columns of \tilde{N} one obtains the diagonal albedo matrix D and the matrix N , whose columns are the normal vectors, such that $ND = \tilde{N}$. The integration of the normal vector field is then performed by one of the approaches described in Section 3.

5. Determining the right surface orientation. As we already observed, the matrices \tilde{N} and L can be determined only up to a unitary transformation Q . It is nevertheless important to suitably choose Q , at least for two reasons.

First of all, the indetermination in the factorization (4.1) may introduce axes reflections in the reference system centered at the object, with the result of capsizing the direction of a part of the normal vectors.

Secondly, the integration procedure in Section 3 assumes that the function describing the shape of the object is single-valued and explicit, that is, has the form $z = u(x, y)$. The matrix Q should introduce a rotation of the reference system which meets this assumption.

As observed in [5], it is impossible to obtain such information from the data, without additional a priori information. In our case, this information comes from the knowledge of the light directions and from a good practice in taking the pictures. The shooting procedure we propose, consists of taking the pictures in a particular order. We assume, conventionally, that for the first picture the light is placed at the right hand of the camera, but this is not restrictive. What is important, is that the light source is moved counterclockwise around the object, in the half space containing the camera, and that the pictures are ordered according to this sequence. There is no need that the light sources are regularly spaced; on this regard, see Remark 4.1.

After determining the matrices $\hat{N} = R^{-T}W$ and $\hat{L} = R^{-T}Z$ by the procedure described in Section 4, we consider the three columns $\hat{\ell}_t$ of \hat{L} , with $t = 1, \lfloor \frac{q}{3} \rfloor, \lfloor \frac{2q}{3} \rfloor$, where $\lfloor x \rfloor$ denotes the integer part of x . Given the above shooting procedure, this vector triplet must have a right-handed (or positive) orientation. This can be checked by the sign of the determinant of the matrix formed by the vector triplet. If the determinant is negative, then the factorization procedure introduced an axis reflection. To restore the original orientation we change the sign of the third row of \hat{N} and \hat{L} , which corresponds to inverting the direction of the z axis.

Once the normal field is well-oriented, we turn to determining a rotation matrix Q that restores the original orientation, i.e., with the camera aligned on the z axis. To approximately identify the direction of the camera as seen from the observed object, given the proposed shooting procedure, we set

$$\mathbf{v}_3 = \sum_{t=1}^q \hat{\ell}_t.$$

and assume the vector \mathbf{v}_3 to be the direction of the z axis. The direction \mathbf{v}_1 of the x axis is arbitrarily obtained by projecting $\hat{\ell}_1$ on the plane orthogonal to \mathbf{v}_3 , and the y axis by computing the cross product $\mathbf{v}_2 = \mathbf{v}_3 \wedge \mathbf{v}_1$. After normalizing the three vectors, the orthogonal matrix

$$Q = [\mathbf{v}_1 \quad \mathbf{v}_2 \quad \mathbf{v}_3]$$

determines the sought rotation, which is used for computing the matrices \tilde{N} and L in (4.4).

6. Numerical experiments. In this section we illustrate the performance of the algorithm for the solution of the photometric stereo problem with unknown lighting discussed in the paper. The Matlab software we developed is available at the web page <http://bugs.unica.it/cana/software/ps3d>. The first two data sets used in the numerical experiments, as well as the reconstructed object of Figure 6.5, are available on the same web page as `mat` files (Matlab data files), and a `ply` 3D model file, respectively. All the computation were performed using Matlab 9.5 on a Debian GNU/Linux system. The 3D meshes displayed in the paper were generated by our software and visualized by the MeshLab open source system for displaying and editing 3D triangular meshes (www.meshlab.net).

The software was tested both with synthetic and experimental data sets, in order to investigate its performance not only when the assumptions on which the algorithm is based are met, but also in a real-world setting, where the assumptions are only approximately verified.

6.1. Synthetic data set. To assess the accuracy attainable by our implementation in the ideal situation when all the assumptions of the method are exactly satisfied, we resorted to a synthetic dataset. We fixed a disposition of $q = 7$ light sources, placing them around the object at angles $(0, \frac{\pi}{4}, \frac{3\pi}{4}, \pi, \frac{5\pi}{4}, \frac{3\pi}{2}, \frac{7\pi}{4})$, and generated a set of digital images by applying the direct model (3.1) to the surface represented by the function

$$u(x, y) = \frac{1}{2}e^x \sin(\pi x) \sin(\pi y), \quad (6.1)$$

on the square domain $[-1, 1] \times [-1, 1]$. Each image is 101×101 pixels, and the albedo equals $\frac{1}{2}$ for $x^2 + y^2 < \frac{1}{4}$, and 1 otherwise. Figure 6.1 and 6.2 show the synthetic surface and the corresponding data set, respectively.

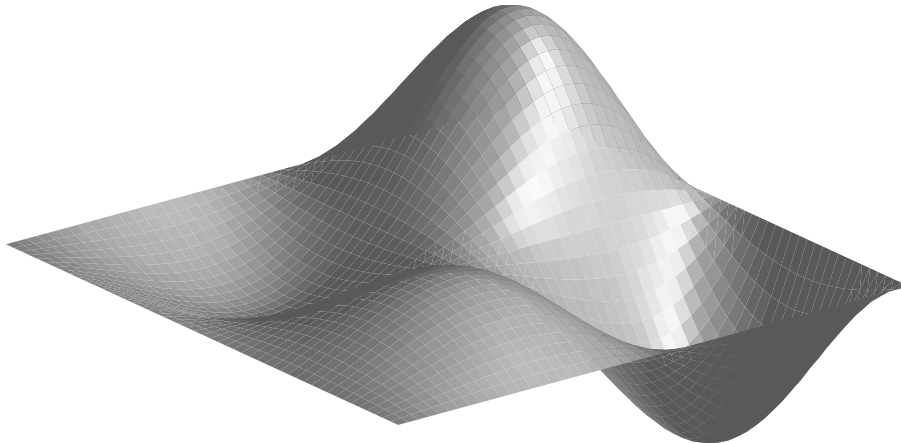


FIGURE 6.1. A synthetic surface used to investigate the performance of the algorithm.

The graph on the left of Figure 6.3 displays the singular values of the data matrix M from (3.3), showing that it clearly has numerical rank 3. Figure 6.4 shows the reconstruction of the light vectors and Figure 6.5 displays the restored surface. The light vectors are recovered up to machine precision, while the relative accuracy on the surface is $2.6 \cdot 10^{-4}$, in accord with the quite large step size $h = \frac{1}{50}$. The two errors are defined by

$$E_{\text{lights}} = \frac{\|L - \tilde{L}\|_F}{\|L\|_F}, \quad E_{\text{surface}} = \frac{\|U - \tilde{U}\|_F}{\|U\|_F},$$

where $\|\cdot\|_F$ is the Frobenius norm, (L, U) denote the exact matrices containing the light vectors and the surface slopes, respectively, and (\tilde{L}, \tilde{U}) the reconstructed matrices.

We repeated the same test after introducing 10% Gaussian noise in the right-hand side M of (3.3). The presence of the noise is reflected in the singular values of M , depicted in the graph

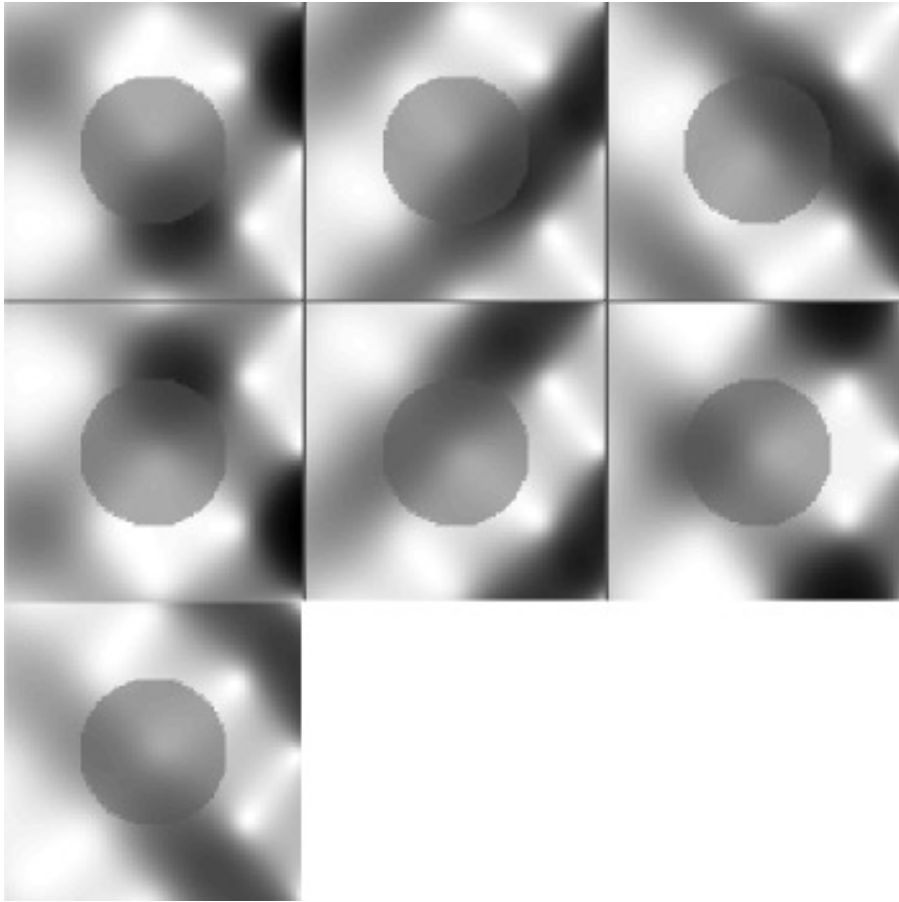


FIGURE 6.2. Data set collected from the synthetic surface displayed in Figure 6.1. It is composed by 7 pictures corresponding to different lighting conditions.

on the right of Figure 6.3. Though its rank is 7, it is evident that M can be well approximated by a rank 3 matrix. The computation is quite steady, as in this case $E_{\text{lights}} = 3.6 \cdot 10^{-3}$, while $E_{\text{surface}} = 1.5 \cdot 10^{-2}$.

The reconstruction in Figure 6.5 was obtained by imposing homogeneous Dirichlet boundary conditions, which are exactly verified by model function (6.1). The error $u(x, y) - \tilde{u}(x, y)$ between the model and the reconstruction is displayed in Figure 6.6. The graph in Figure 6.7 shows the error corresponding to exact Neumann conditions. In this case we fixed the value of the solution at the central point of the domain, that is, $\gamma = u(0, 0) = 0$; see Remark 3.1. Neumann conditions produced a less accurate reconstruction in proximity of the border of the domain, compared to Dirichlet conditions.

To investigate how deviation from ideal lighting influences numerical results, we repeated the above experiment, with Dirichlet conditions and without noise, positioning the light sources at finite distance κA from the object, where κ is a scale factor and A is the horizontal width of the observed scene; in this particular example $A = 2$. The synthetic images were generated by a model based on Lambert's law, which considers incident light rays, rather than parallel rays. The light directions were recovered by the procedure described in Section 4.

When $\kappa < \infty$ the matrix M in (3.4) is full-rank, and this deteriorates the approximation accuracy of the rank-3 factorization constructed in Section 4. We measure the closeness of the matrix M to being rank-3 by the ratio σ_3/σ_4 between the third and the fourth singular value of M . Table 6.1 reports this ratio together with the errors E_{lights} and E_{surface} , for values of κ ranging from ∞ to 1. For example, when $\kappa = 10$ the distance of the light source from the origin is 10

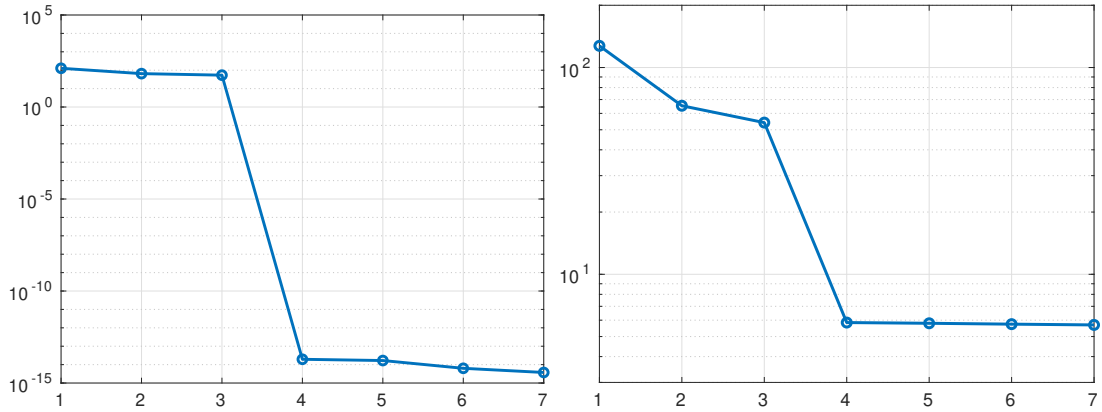


FIGURE 6.3. On the left, singular values of the data matrix M for the synthetic data set; on the right, singular values of the same matrix after 10% Gaussian noise is added.

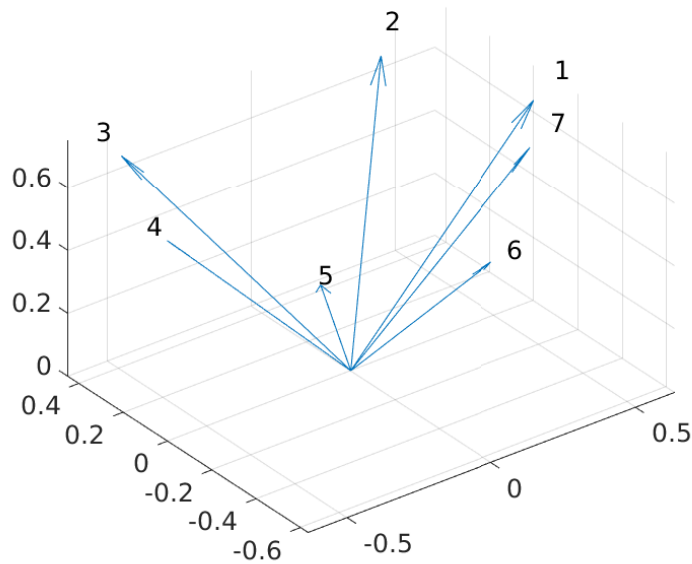


FIGURE 6.4. Reconstruction of the light directions.

times the width of the observed scene.

It is immediate to observe that when κ takes value close to 1, the error produced in the light directions is amplified in the object reconstruction, leading to unacceptable results. We observed that the algorithm may fail in some situation, as the deviation from ideality can lead to a non positive definite matrix G in (4.3), causing an unrecoverable error. This is one of the drawbacks of the numerical method, that must be faced in future research.

6.2. Experimental data sets. An experimental data set partially satisfying the assumptions required by the reconstruction method was generated as follows. A seashell (approximate width 10 cm) was placed face up on a horizontal desk with a black background. The camera was held by a tripod about 1 m above the seashell. The flat background was intended to reproduce homogeneous Dirichlet boundary conditions for the observed surface. The desk, standing in the open air under direct sunlight, was rotated in order to take 20 pictures of the seashell with different lighting directions, according to the shooting procedure described in Section 5. The resulting data

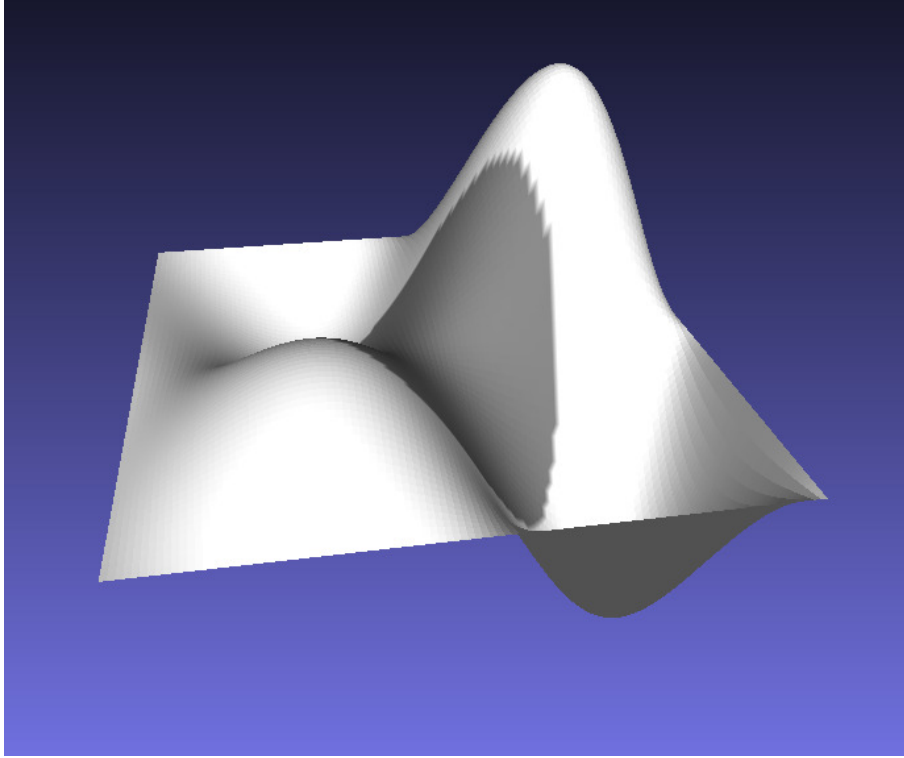


FIGURE 6.5. Restored surface.

TABLE 6.1

Influence of the distance between the object and the light source: the unit for the distance κ is the scene width, the ratio σ_3/σ_4 represents “closeness to rank 3”, the errors are relative in the Frobenius norm.

κ	σ_3/σ_4	E_{lights}	E_{surface}
∞	$1.85 \cdot 10^{15}$	$1.00 \cdot 10^{-15}$	$2.69 \cdot 10^{-4}$
1000	$2.19 \cdot 10^3$	$1.95 \cdot 10^{-4}$	$1.39 \cdot 10^{-3}$
100	$2.18 \cdot 10^2$	$1.95 \cdot 10^{-3}$	$1.41 \cdot 10^{-2}$
10	$2.15 \cdot 10^1$	$1.95 \cdot 10^{-2}$	$1.45 \cdot 10^{-1}$
1	1.77	$4.52 \cdot 10^{-1}$	3.89

set is displayed in Figure 6.8.

While the relatively small distance between the camera and the object produces images which cannot be represented through the orthographic projection model, the sunlight rays can be assumed to be parallel. So the lighting verifies the assumption of Lambert’s model and we expect the data matrix M to be approximately rank-3.

The digital pictures were recorded in *raw* mode at the resolution of 3477×5220 pixels, and for this particular numerical simulation they were scaled to 885×705 pixels. The procedure described in Sections 4 and 5 identified 20 light vectors, displayed in Figure 6.9, that are compatible with the sunlight position during the shooting process.

By solving the Poisson equation (3.6) with homogeneous Dirichlet boundary conditions, one obtains the 3D model illustrated in Figure 6.10 by two different views. Compared to the original, the model appears slightly deformed by the deviation from the orthographic projection model, but the reconstruction is quite accurate and the computing time negligible, 2.8 seconds on an Intel Core i7 computer. The deformation induced by the camera system could be corrected by camera calibration techniques.

As a second experiment based on a real data set, we processed the images of a stela of the

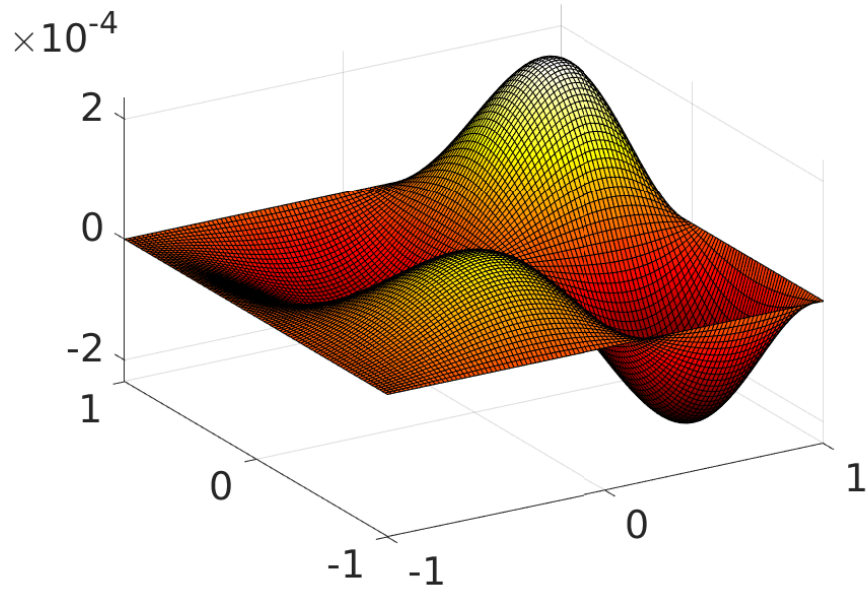


FIGURE 6.6. *Reconstruction error with Dirichlet boundary conditions.*

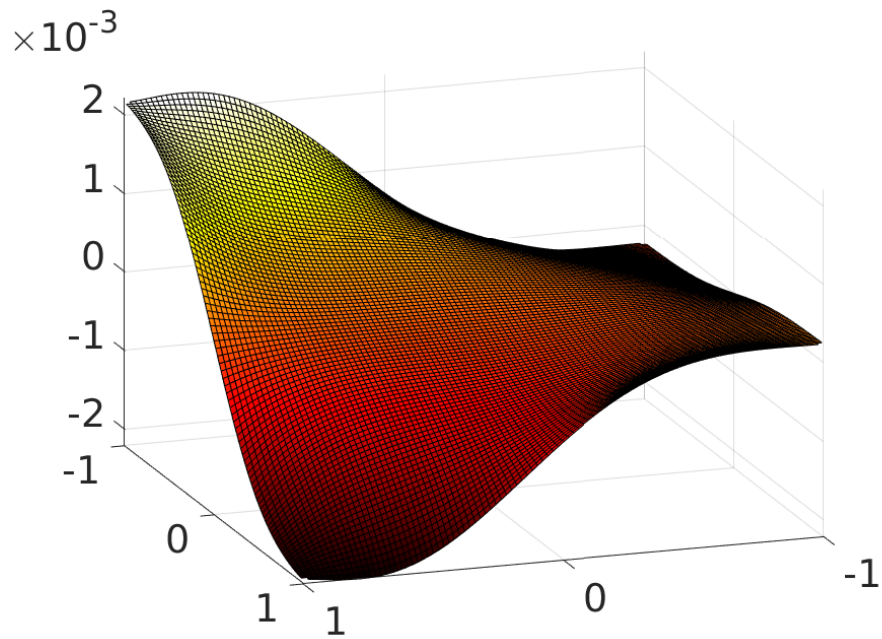


FIGURE 6.7. *Reconstruction error with Neumann boundary conditions.*

Ptolemaic period, exhibited at the Museo Egizio in Torino, Italy (<https://www.museoegizio.it>); see Figure 6.11. We thank the Museo Egizio, in particular Christian Greco, director of the museum, and Marco Rossani, collection manager, for providing us the data set, which is composed by 8 images. A black mask was added around the stela in each image, in order to reproduce Dirichlet boundary conditions. The resolution of the *raw* digital pictures is 7360×4912 pixels. The images were scaled to 1474×2208 pixels to produce the result depicted on the right of Figure 6.11, where

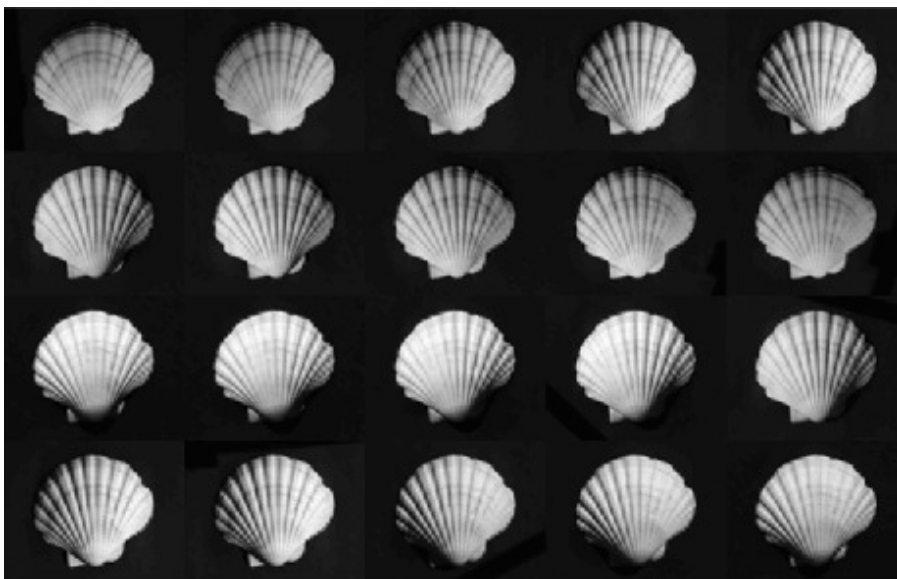


FIGURE 6.8. *The SHELL data set, consisting in 20 images corresponding to different sunlight directions.*

the surface is displayed after removing the albedo. The computation took 16 seconds.

The pictures were taken in the exposition room of the museum using an electronic flash as a light source, so they do not satisfy the assumptions of the model, being both the camera and the light source at a quite small distance from the object. Indeed, while the bas-relief details are accurately reproduced, the reconstructed surface is spherically warped, compared to the flatness of the real stela.

Some details of the reconstructed surface are displayed in Figure 6.12. The left and central pictures show how albedo removal can lead to a cleaner visualization of an engraving. The image on the right is a part of the reconstruction obtained by processing a 800×800 sub-image of the original high resolution pictures. It shows a writing, located in the central part of the stela. To obtain a neat representation of small writings one would need high resolution images only of this part, but this would introduce difficulties in assigning boundary conditions to the Poisson equation. We will face this problem in future work.

7. Conclusions and future perspectives. In this paper, under the ideal assumptions upon which Lambert's model is based, we investigate the performance of the Hayakawa [16] method for estimating the lights position in photometric stereo. This procedure can be applied when at least 6 images of an object are available, each one with a different light source. We show that this approach can be effectively used to reconstruct the 3D model of an observed object, and we propose a procedure to avoid the indetermination in the direction of the normal vectors, typical of photometric stereo. We also make available the software we developed.

The accuracy of our method is investigated through numerical experiments on both synthetic and real data sets. Our experiments show that the algorithm is accurate under ideal conditions, and that the lack from ideality produces, as expected, a spherical deformation on the reconstructed surfaces.

Our future research work will be devoted to improving the method, in order to make it applicable to real shooting conditions, in particular when the light sources cannot be positioned sufficiently far away from the observed object. Moreover, real time processing of high resolution pictures requires a reduction in the computing time, especially for what concerns the data matrix factorization and the solution of the final large linear system. Another aspect that needs further work is the treatment of the boundary conditions required for the solution of equation (3.6), whose knowledge is not available in many applicative situations.

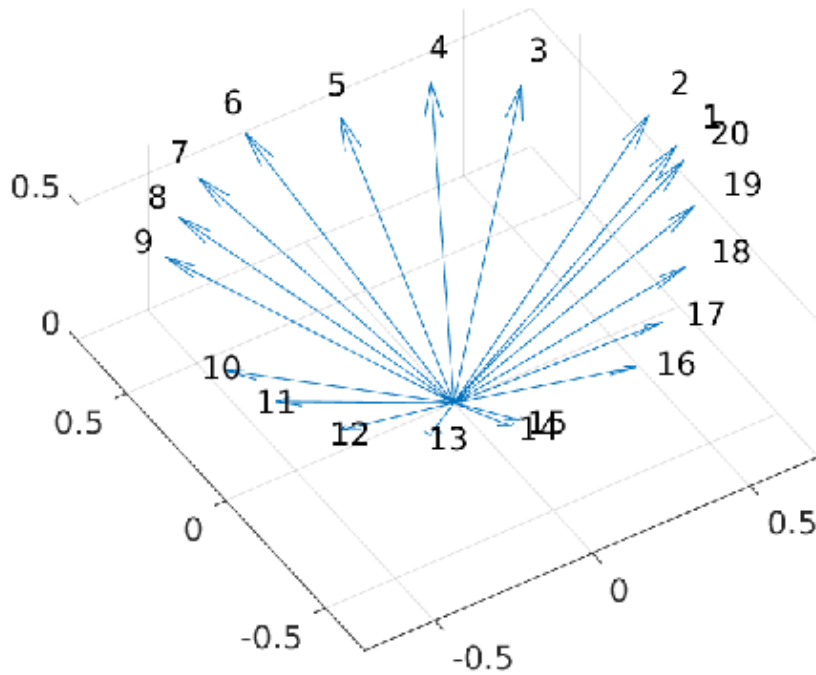


FIGURE 6.9. Light directions identified by the reconstruction algorithm for the SHELL data set.

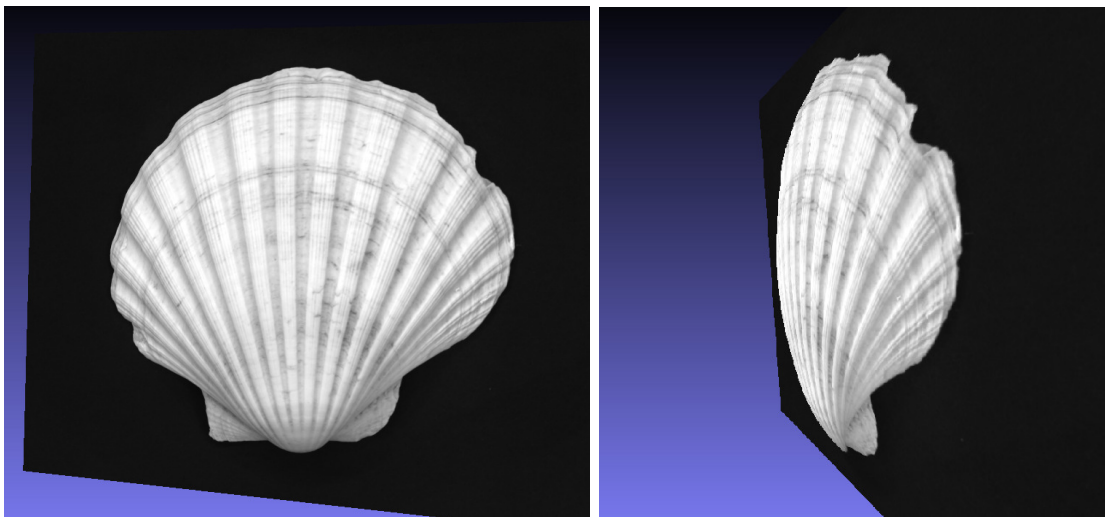


FIGURE 6.10. Two different views of the 3D surface reconstructed from the SHELL data set.

Acknowledgment. We thank the Museo Egizio (Torino, Italy) for providing us the data set used in the numerical experiments. The research in this paper was partially supported by the Fondazione di Sardegna 2017 research project “Algorithms for Approximation with Applications [Acube]”, the INdAM-GNCS research project “Tecniche numeriche per l’analisi delle reti complesse e lo studio dei problemi inversi”, and the Regione Autonoma della Sardegna research project “Algorithms and Models for Imaging Science [AMIS]” (RASSR57257, intervento finanziato con risorse FSC 2014-2020 - Patto per lo Sviluppo della Regione Sardegna). AC and CF gratefully



FIGURE 6.11. On the left, stela in honor of the general Callimachos, mentioning Cleopatra and Caesarion; granite, Ptolemaic period, reign of Cleopatra VII, 39 BC. Thebes, Temple of Karnak (Courtesy of Museo Egizio, Torino, Italy). On the right, 3D reconstruction obtained by the algorithm described in the paper.

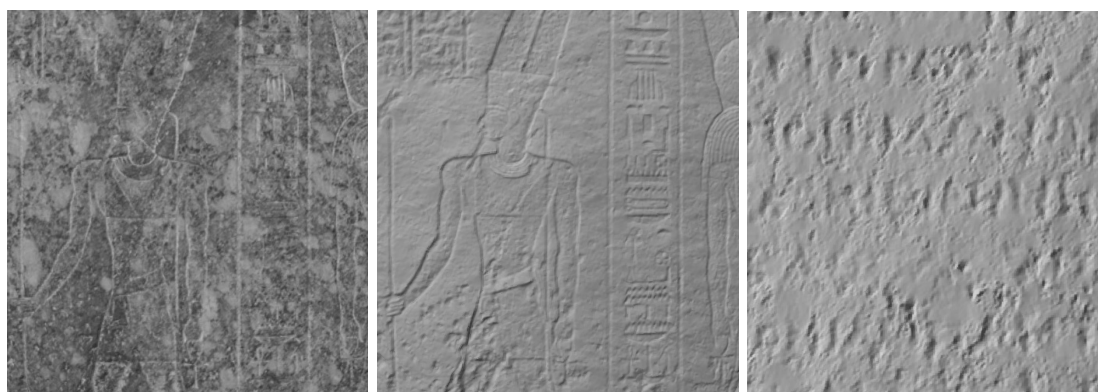


FIGURE 6.12. Three details of the Ptolemaic stela reconstruction: the first two show the same area with and without albedo, the third one a part containing a writing.

acknowledge Regione Autonoma della Sardegna for the financial support provided under the Operational Programme P.O.R. Sardegna F.S.E. (European Social Fund 2014-2020 - Axis III Education and Formation, Objective 10.5, Line of Activity 10.5.12).

REFERENCES

- [1] J. Baglama and L. Reichel. Augmented implicitly restarted Lanczos bidiagonalization methods. *SIAM J. Sci. Comput.*, 27:19–42, 2005.
- [2] J. Baglama and L. Reichel. An implicitly restarted block Lanczos bidiagonalization method using Leja shifts. *BIT*, 53:285–310, 2013.
- [3] S. Barsky and M. Petrou. The 4-source photometric stereo technique for three-dimensional surfaces in the presence of highlights and shadows. *IEEE Trans. Pattern Anal. Mach. Intell.*, 25(10):1239–1252, 2003.
- [4] R. Basri, D. Jacobs, and I. Kemelmacher. Photometric stereo with general, unknown lighting. *Int. J. Comput.*

- Vis.*, 72(3):239–257, 2007.
- [5] P. N. Belhumeur, D. J. Kriegman, and A. L. Yuille. The bas-relief ambiguity. *Int. J. Comput. Vis.*, 35(1):33–44, 1999.
- [6] Å. Björck. *Numerical Methods for Least Squares Problems*. SIAM, Philadelphia, 1996.
- [7] B. L. Buzbee, G. H. Golub, and C. W. Nielson. On direct methods for solving Poisson’s equations. *SIAM Journal Numer. Anal.*, 7(4):627–656, 1970.
- [8] T. F. Chan and D. C. Resasco. A domain-decomposed fast Poisson solver on a rectangle. *SIAM J. Sci. Stat. Comput.*, 8(1):s14–s26, 1987.
- [9] C.-P. Chen and C.-S. Chen. The 4-source photometric stereo under general unknown lighting. In *Computer Vision–ECCV 2006*, pages 72–83. Springer, Vienna, 2006.
- [10] P. H. Christensen and L. G. Shapiro. Three-dimensional shape from color photometric stereo. *Int. J. Comput. Vis.*, 13(2):213–227, 1994.
- [11] R. Dessì. Algoritmi Ottimizzati per la Photometric Stereo Applicati all’Archeologia. Bachelor’s Thesis in Electrical Engineering, University of Cagliari. Available at <http://bugs.unica.it/~gppe/did/tesi/14dessi.pdf>, 2014.
- [12] R. Dessì, C. Mannu, G. Rodriguez, G. Tanda, and M. Vanzi. Recent improvements in photometric stereo for rock art 3D imaging. *Digital Applications in Archaeology and Cultural Heritage (DAACH)*, 2:132–139, 2015.
- [13] C. R. Dyer. Volumetric scene reconstruction from multiple views. In *Foundations of Image Understanding*, pages 469–489. Springer, Vienna, 2001.
- [14] P. Floris. Photometric Stereo e Archeologia. Bachelor’s Thesis in Electrical and Electronical Engineering, University of Cagliari. Available at <http://bugs.unica.it/~gppe/did/tesi/17floris.pdf>, 2017.
- [15] G. H. Golub and C. F. Van Loan. *Matrix Computations*. The John Hopkins University Press, Baltimore, third edition, 1996.
- [16] H. Hayakawa. Photometric stereo under a light source with arbitrary motion. *J. Opt. Soc. Am. A-Opt. Image Sci. Vis.*, 11(11):3079–3089, 1994.
- [17] B. K. P. Horn. Obtaining shape from shading information. In *Shape from Shading*, pages 123–171. MIT Press, 1989.
- [18] R. Klette, K. Schlüns, and A. Koschan. *Computer Vision: Three-dimensional Data from Images*. Springer, Singapore, 1998.
- [19] R. Kozera. Existence and uniqueness in photometric stereo. *Appl. Math. Comput.*, 44(1):1–103, 1991.
- [20] C. Mannu. 3D Photometric Stereo per l’Arte Preistorica. Bachelor’s Thesis in Electrical and Electronical Engineering, University of Cagliari. Available at https://www.academia.edu/8502503/3D_Photometric_Stereo_per_lArte_Preistorica, 2014.
- [21] C. Mannu, G. Rodriguez, G. Tanda, and M. Vanzi. Nuovi sviluppi nelle tecniche di stereofotometria 3D di incisioni e rilievi. applicazioni nella tomba XV di Sos Furrighesos, Sardegna. In F. Troletti, editor, *Prospects for the Prehistoric Art Research, 50 Years Since the Founding of Centro Camuno. Proceedings of the XXVI Valcamonica Symposium, September 9–12, 2015*, pages 285–288, Capo di Ponte, Italy, 2015. Centro Camuno di Studi Preistorici. ISBN: 978-1-4673-1159-5.
- [22] C. Mannu, G. Rodriguez, and M. Vanzi. Rilievo 3D non a contatto: tecniche speciali per l’arte rupestre. In G. Tanda, editor, *Nuove Tecniche di Documentazione e di Analisi per una Ricostruzione delle Società dalla Fine del V al III Millennio a.C., Volume II*, chapter II, pages 37–52. Edizioni Condaghes, Cagliari, Italy, 2016. ISBN: 978-88-7356-231-3.
- [23] The MathWorks, Inc., Natick, MA. *Matlab ver. 8.4*, 2014.
- [24] R. Mecca and J.-D. Durou. Unambiguous photometric stereo using two images. In *International Conference on Image Analysis and Processing*, pages 286–295. Springer, 2011.
- [25] R. Mecca and M. Falcone. Uniqueness and approximation of a photometric shape-from-shading model. *SIAM J. Imaging Sci.*, 6:616–659, 2013.
- [26] G. Slabaugh, B. Culbertson, T. Malzbender, and R. Schafer. A survey of methods for volumetric scene reconstruction from photographs. In *Proceedings of the 2001 Eurographics Conference on Volume Graphics*, pages 81–100, Vienna, 2001. Springer.
- [27] G. Stocchino. Modelli Matematici e Algoritmi Numerici per la Photometric Stereo. Bachelor’s Thesis in Mathematics, University of Cagliari. Available at <http://bugs.unica.it/~gppe/did/tesi/15stocchino.pdf>, 2015.
- [28] M. Vanzi, C. Mannu, R. Dessì, G. Rodriguez, and G. Tanda. Photometric stereo for 3D mapping of carvings and reliefs: case studies on prehistorical art in Sardinia. In *XVII Seminário Internacional de Arte Rupestre de Mação*, volume Visual Projections N. 3, Mação, Portugal, 2014. Ângulo Repositório Didáctico (ISSN 1645-8214).
- [29] R. J. Woodham. Photometric method for determining surface orientation from multiple images. *Opt. Eng.*, 19(1):191139–191139, 1980.